

Modular Deep-Learning-Based Early Warning System for Deadly Heatwave Prediction

Shangqing Xu^{1*}, Zhiyuan Zhao¹, Megha Sharma¹, José María Martín-Olalla²,
Alexander Rodríguez³, Gregory A. Wellenius⁴, B. Aditya Prakash^{1*}

¹College of Computing, Georgia Institute of Technology, Atlanta, GA, USA.

²Departamento de Física de la Materia Condensada, Facultad de Física, Universidad de Sevilla, Sevilla, Spain.

³Computer Science and Engineering, University of Michigan, Ann Arbor, MI, USA.

⁴Department of Environmental Health, School of Public Health, Boston University, Boston, MA, USA.

*Corresponding authors. Email: sxu452@gatech.edu, badityap@cc.gatech.edu

Severe heatwaves in urban areas significantly threaten public health, calling for establishing early warning strategies. Despite predicting occurrence of heatwaves and attributing historical mortality, predicting an incoming deadly heatwave remains a challenge due to the difficulty in defining and estimating heat-related mortality. Furthermore, establishing an early warning system imposes additional requirements, including data availability, spatial and temporal robustness, and decision costs. To address these challenges, we propose **DEEPTHERM**, a modular early warning system for deadly heatwave prediction without requiring heat-related mortality history. By highlighting the flexibility of deep learning, **DEEPTHERM** employs a dual-prediction pipeline, disentangling baseline mortality in the absence of heatwaves and other irregular events from all-cause mortality. We evaluated **DEEPTHERM** on real-world data across Spain. Results demonstrate consistent, robust, and accurate performance across diverse regions, time periods, and population groups while allowing trade-off between missed alarms and false

alarms.

1 Introduction

Severe heatwaves, characterized by consecutive days of extremely high temperatures (1, 2, 3), are a significant driver of excess mortality in urban areas and pose a major threat to public health (4, 5, 6, 7). For instance, the 2003 European heatwave caused over 40,000 deaths (8), including approximately 2,000 in the Netherlands (9) and 3,000 in Spain (10). Mitigating the impact of these events necessitates their accurate prediction and the development of effective early warning systems (11).

Although extensive research has focused on predicting the occurrence of high temperatures (12, 13, 14, 15) or attributing historical mortality to heat (6, 16, 17, 18), forecasting whether an incoming heatwave will be deadly or not remains a significant challenge (19, 7). A primary obstacle lies in the difficulty of obtaining suitable data. An accurate deadly heatwave prediction model requires data on excess mortality—the number of deaths above a baseline level that are attributable to heat—but this metric is complex to define and estimate precisely (18, 7). Official records typically only provide all-cause mortality, which combines this desired excess mortality with baseline mortality (deaths from other causes). This fundamental data limitation complicates the development of reliable deadly heatwave predictors.

Among all the existing progress around deadly heatwaves, only a few approaches propose to circumvent the challenge of acquiring direct heat-related mortality data. The proposed methods include projecting non-mortality variables such as meteorology and population demographics to predict future excess mortality (20), or utilizing long-term-averaged mortality as a reference value (21). Yet, they both suffer from key limitations. First, by only modeling the relationship from non-mortality variables or long-term averages to daily mortality in the future, they cannot utilize the rich predictive information contained within daily historical mortality data. Second, these models still require ground-truth excess mortality data for calibration and evaluation, which, as previously established, is difficult to obtain in practice.

Beyond the initial excess mortality prediction, implementing an effective early warning system for deadly heatwaves presents further practical challenges. First, since the system's outputs are designed to inform policy decisions, the model must be optimized to balance the significant costs

associated with both false alarms and missed detections (22, 23, 24). Second, the system must be robust and generalizable, maintaining its reliability when deployed in different regions or as new data becomes available. This transportability is crucial for its broader application and impact (25).

In summary, developing an early warning system for deadly heatwave classification presents multiple challenges: (1) the inherent difficulty of predicting deadly heatwaves among all incoming heatwaves due to a lack of heat-related mortality data, and (2) the requirements of data availability, robustness, and consideration of decision-related risks. Existing early warning systems for heatwaves remain limited to categorizing heatwaves by applying temperature thresholds derived from historical temperature-mortality relationships (26, 27, 28, 29, 30). To the best of our knowledge, no existing studies have developed or validated early warning systems to reveal the presence of deadly heatwaves based on mortality predictions.

To tackle these challenges, we propose a novel dual-prediction strategy to address the challenge of data scarcity. Our approach concurrently predicts two quantities: (1) all-cause mortality and (2) baseline mortality (i.e., mortality in the absence of irregular events like heatwaves). This strategy is motivated by the observation that baseline mortality is far less sensitive to short-term factors, such as daily weather, than all-cause mortality, which has been leveraged by previous mortality attribution studies (31, 32). Accordingly, we propose to use a simpler model trained on long-term historical data to capture the stable baseline mortality, while a more complex model uses short-term records and non-mortality factors to predict the all-cause mortality. The difference between these two predictions yields an estimate of excess mortality. Although this value may include effects from other non-heat-related events, it serves as a robust proxy for identifying and classifying deadly heatwaves. Inside such a design, predicting all-cause mortality requires analyzing the complex relationship between mortality and non-mortality variables. Therefore, we propose to introduce deep-learning-based models as the all-cause predictor, leveraging their strong capabilities in complex sequence prediction (33, 34).

Based on our dual-prediction strategy, we establish **DEEPTHERM**, a modular early warning system for deadly heatwaves, as illustrated in Figure 1. **DEEPTHERM** is composed of three key components: (1) a deep learning module that forecasts all-cause mortality; (2) a Quasi-Poisson regression module that predicts baseline mortality, thereby enabling the estimation of excess mortality; and (3) a decision module that uses this estimate to classify whether a heatwave qualifies as

deadly. The deep-learning-based prediction module is expected to accurately predict the all-cause mortality data given historical all-cause mortality data and historical non-mortality data, which is accessible in most regions through national agencies—ensuring broad temporal applicability. Furthermore, we introduce synoptic weather-typing data that categorize weather patterns linked to heatwave occurrences (2, 35). Due to advances in synoptic prediction systems (36, 37, 38, 39), these data are widely available for the near-future, and we therefore incorporate their outputs in DEEPTHERM as references for future heatwave occurrences. Additionally, DEEPTHERM employs a flexible thresholding strategy for issuing deadly heatwave alarms, allowing adjustments based on varying tolerance levels for false alarms versus missed detections.

We evaluated DEEPTHERM’s performance across 12 provinces of Spain (2015–2023) and their corresponding capital cities (1995–2023). In each city and province, we assess DEEPTHERM in a *real-time* manner: on each day t , we train DEEPTHERM with all available non-mortality and mortality data up to day t and synoptic weather-typing data up to day $t + 5$ to give deadly heatwave predictions from day $t + 1$ to day $t + 5$. DEEPTHERM processes daily non-mortality variables (e.g., temperature, humidity, and wind speed) alongside historical all-cause mortality data to classify heatwaves into three categories: level 0, 1, and 2, based on how much the heat-related mortality accounts for in the all-cause mortality. This categorization setting allows us to quantify DEEPTHERM’s performance under broader or stricter definitions of deadly heatwaves. Our results demonstrate that DEEPTHERM achieves: 80% detection rate for level 1 heatwaves with a less than 15% false alarm rate, and 60% detection rate for level 2 heatwaves with a 25% false alarm rate. Moreover, the system exhibits consistent robustness across different age groups (including younger and older populations), evaluation years, and geographic regions with varying climate conditions. Furthermore, we show that DEEPTHERM supports customizable alarm thresholds, enabling policymakers to balance the trade-offs between missed alarms and false alarms according to operational needs.

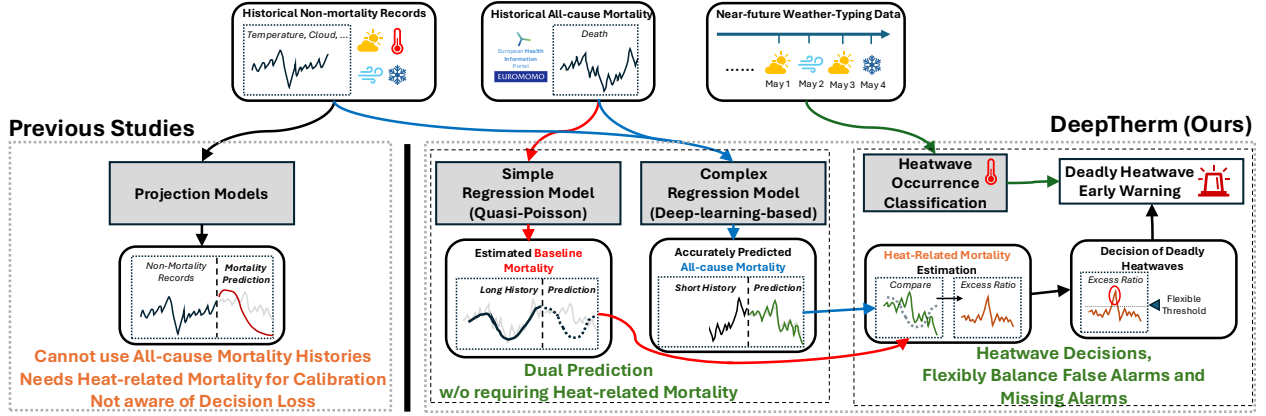


Figure 1: DEEPTherm is capable of using all-cause mortality history with non-mortality records to yield early warnings for deadly heatwaves. Existing studies of deadly heatwaves remain on projecting non-mortality variables to heat-related mortality, which cannot use historical all-cause mortality records and need heat-related mortality for calibration. Our system, DEEPTherm, bypasses this challenge with a novelly proposed dual-prediction pipeline. Using historical all-cause mortality data, historical non-mortality data, and near-future synoptic weather-typing data, DEEPTherm isolates heat-related and baseline mortality components, enabling deadly heatwave identification without requiring heat-related mortality data. Furthermore, DEEPTherm determines whether an incoming heatwave will be deadly via a flexible thresholding strategy, capable of balancing false alarms and missed alarms.

2 Results

2.1 Experiment Settings

For a multi-day heatwave, if heat-related mortality exceeds 15% of baseline mortality on any day, we classify it as a Level 1 (L1) heatwave; and if heat-related mortality exceeds 30% of baseline mortality on any day, we further classify it as a Level 2 (L2) heatwave; otherwise, the heatwave is categorized as a Level 0 heatwave. Given the time series of historical all-cause mortality and non-mortality data for a given location, DEEPTherm predicts for each incoming heatwave: 1) whether it will surpass *Level 1*, and 2) whether it will surpass *Level 2*. The occurrence of incoming heatwaves is predicted by synoptic weather-typing data, where we choose Spatial Synoptical Classifications (36) (Details shown in Section 4.2).

To ensure sufficient training data, we begin the evaluation from the third year in each city/province. Additionally, to reduce computational costs, we update mortality predictors annually while retaining the previous year’s weights for the all-cause mortality predictor. Meanwhile, to maintain the accuracy of the baseline mortality predictor, we re-train the Quasi-Poisson model from scratch each year using only the two most recent years’ data, as population changes over time would otherwise alter the distribution of baseline mortality. By default, we maintain thresholds of DEEPTHERM in 15% for L1 heatwaves and 30% for L2 heatwaves throughout the study. The sources of data can be found in Section 4.1. Original result tables will be shown in Supplementary.

2.2 Spatial Robustness: Performance across Cities and Provinces

To demonstrate the overall performance of DEEPTHERM in each city and province, we show the evaluation results aggregated over the entire study period in Table 1, along with the performance of baseline methods for comparison. The results are shown in four metrics: 1) Accuracy, 2) Precision, 3) Recall, and 4) F1-score. We show the definition of metrics in Supplementary. Intuitively, higher precision indicates fewer false alarms (i.e., fewer false positives); Higher recall reflects fewer missed alarms (i.e., fewer false negatives); Higher accuracy signifies better overall correctness in labeling heatwaves (deadly or not); Higher F1-score suggests a balanced reduction in both false and missed alarms. Additionally, Figure 2 visualizes the spatial distribution of prediction accuracies.

For provincial L1 heatwave prediction (Table 1a), DEEPTHERM achieved an average accuracy of 77.0%, with 80.6% precision, 87.4% recall, and 83.8% F1-score. These results indicate that, over 17 out of 20 issued alarms corresponded to actual L1 heatwaves, over 16 out of 20 L1 heatwaves were detected, and over 15 out of 20 model predictions were correct. Performance for L2 heatwave prediction was slightly lower, with 66.4% accuracy, 55.6% precision, 64.8% recall, and 59.8% F1-score. These results indicate that, approximately 11 out of 20 issued alarms corresponded to actual L2 heatwaves, around 13 out of 20 L2 heatwaves were detected, and roughly 13 out of 20 predictions were correct.

Notably, in provinces experiencing more than three heatwaves annually (e.g., Madrid, Seville, Zaragoza, Córdoba, and Badajoz), DEEPTHERM achieved higher performance for L1 heatwave prediction (Table 1a), with an average precision of 84.6% and recall of 89.0%, surpassing results in

	City	Alicante	Badajoz	Barcelona	Biscay	Cordoba	Madrid	Malaga	Orense	Seville	Toledo	Valencia	Zaragoza	Total
L1	Acc.	100.0	87.8	50.0	50.0	84.9	80.0	76.9	83.3	79.0	72.7	88.9	68.4	77.0
	Pr.	50.0	88.6	66.7	100.0	91.9	84.4	85.7	83.3	82.9	100.0	85.7	75.0	80.6
	Rec.	100.0	97.5	66.7	100.0	87.2	84.4	75.0	100.0	90.2	70.0	100.0	85.7	87.4
	F1	100.0	92.9	66.7	66.7	89.5	84.4	80.0	50.9	86.4	82.4	92.3	80.0	83.8
L2	Acc.	100.0	57.1	50.0	50.0	73.6	68.0	76.9	66.7	69.4	45.5	44.4	57.9	65.1
	Pr.	-	57.6	0.0	-	73.9	42.9	25.0	75.0	66.7	37.5	40.0	63.6	58.3
	Rec.	-	73.1	0.0	0.0	68.0	42.9	100.0	75.0	84.2	75.0	50.0	63.6	67.3
	F1	-	64.4	-	-	70.8	42.9	40.0	75.0	74.4	50.0	44.4	63.6	62.4

(a) Scores across all areas in classifying provincial heatwaves

	City	Alicante	Badajoz	Barcelona	Bilbao	Cordoba	Madrid	Malaga	Orense	Seville	Toledo	Valencia	Zaragoza	Total
L1	Acc.	78.6	76.8	77.8	66.7	82.3	68.1	61.9	70.0	73.5	76.0	88.9	80.0	74.9
	Pr.	90.0	82.5	100.0	66.7	82.6	68.0	64.7	70.0	78.7	86.4	92.9	90.2	78.7
	Rec.	81.8	91.2	71.4	100.0	97.9	86.7	84.6	100.0	87.6	86.4	92.9	84.1	89.6
	F1	85.7	86.7	83.3	80.0	89.6	76.2	73.3	82.4	82.9	86.4	92.9	87.1	83.8
L2	Acc.	78.6	72.5	66.7	83.3	66.9	75.9	66.7	40.0	63.6	68.0	77.8	63.6	69.2
	Pr.	80.0	81.5	66.7	100.0	69.6	47.8	50.0	37.5	61.7	66.7	80.0	73.1	66.6
	Rec.	88.9	83.0	50.0	75.0	83.1	64.7	71.4	75.0	59.7	93.3	57.1	59.4	73.1
	F1	84.2	82.2	57.1	85.7	75.7	55.0	58.8	50.0	60.7	77.8	66.7	65.5	69.7

(b) Scores across all cities in classifying city-level heatwaves

Table 1: DEEPTherm consistently performs in cities and provinces located across Spain, both in classifying L1 heatwaves and L2 heatwaves. Tables summarize DEEPTherm’s prediction results for (a) provincial and (b) city-level heatwaves, including: 1) Accuracy (Acc.), 2) Precision (Pr.), 3) Recall (Rec.), and 4) F1 score (definitions are provided in the Supplementary Materials). All values are reported as percentages. On average, DEEPTherm achieves approximately 75% Precision and 85% Recall for L1 heatwaves, and 55% Precision and 65% Recall for L2 heatwaves. It misses fewer than 5 out of 20 L1 heatwaves and 7 out of 20 L2 heatwaves, while generating only 3 false alarms for L1 and 7 for L2 out of 20 alarms. The model’s robust performance across cities and provinces under diverse climate conditions confirms its ability to effectively capture the relationship between non-mortality data and all-cause mortality.

other provinces (81.6% precision, 87.4% recall). This disparity was even more pronounced for L2 heatwave prediction: high-frequency provinces attained 60.9% precision and 66.4% recall, while others showed lower precision (44.4%) but higher recall (75.0%). Yet, this trend is not observed

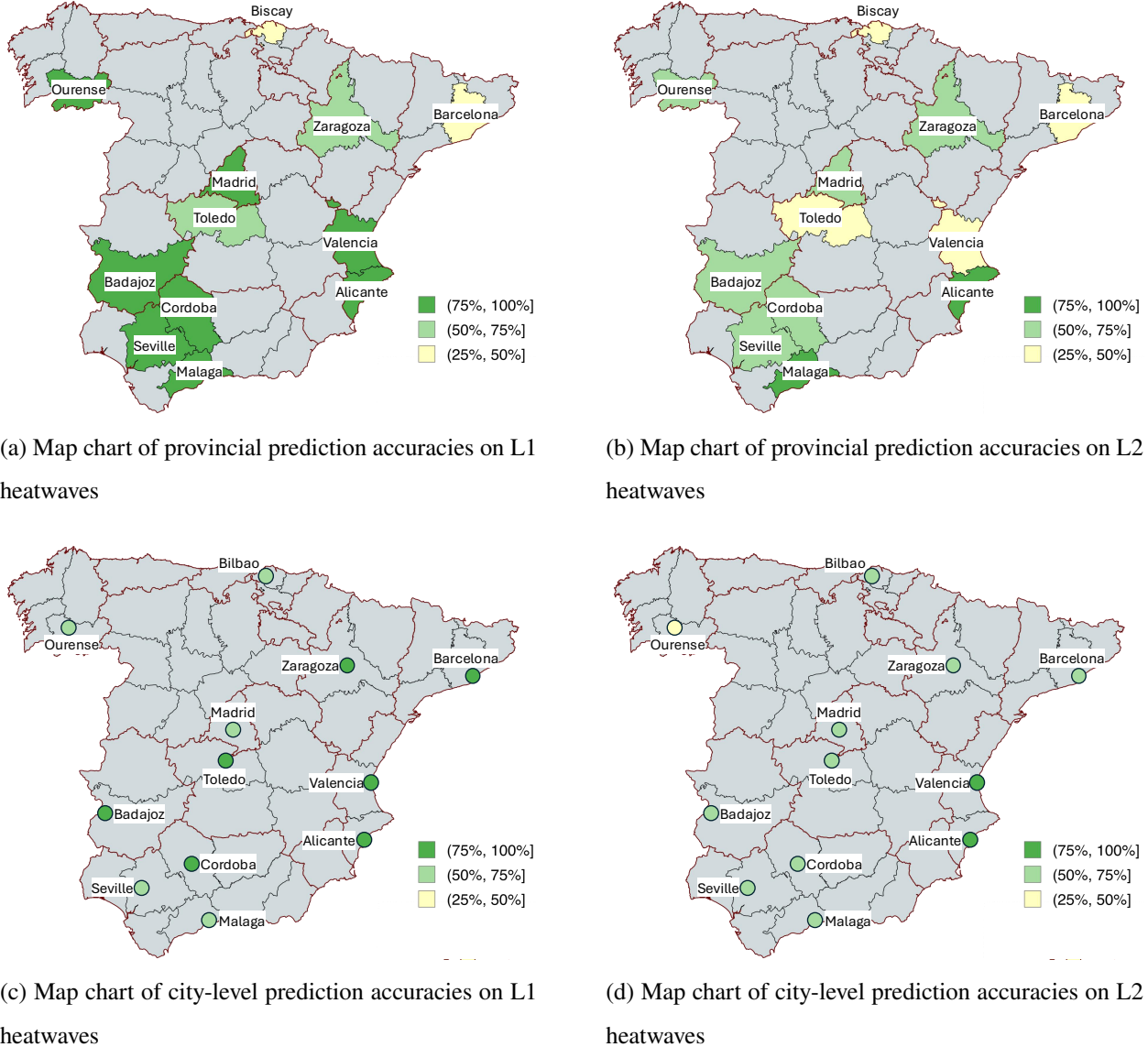


Figure 2: A visualization of DEEPTherm’s performance on Spain (mainland). Figure (a) (b) shows the map chart noting the provincial prediction accuracies, and Figure (c) (d) notes the city-level prediction accuracies. Provinces outside Iberian Peninsula are hidden for brevity.

in city-level predictions (Table 1b), where most of the cities are equipped with plenty of heatwave records. In the deadly prediction on the five aforementioned cities, DEEPTherm received 80.4% precision and 89.5% recall, close to the other cities (81.5% precision, 88.2% recall). Similarly, in L2 heatwave predictions, DEEPTherm received 66.7% precision and 70.0% recall, which is lower than the other cities (68.7% precision, 73.0% recall).

2.3 Temporal Robustness: Performance across Different Years

To demonstrate the temporal variance of DEEPTHERM’s performance, we summarize the precision and recall of city-level L1 heatwave prediction results year-by-year. As shown in Figure 3, the model receives 100 percent precision and recall (meaning all heatwaves are correctly classified) on more recent years, but the performance falls more in earlier years, especially before 2005. Among all years, the prediction result in 2016 is the best, with all 7 cities with heatwaves receiving over 80% precision and recall. The worst prediction result comes from the years 2020 and 2021, where approximately 3 out of 10 cities with heatwaves received precision and recall lower than 70%. An intuitive answer to this drop might be the occurrence of the COVID-19 pandemic, which we discuss in more detail later. It is also worth mentioning that the trends in precision and recall over time are stable in the Continental area, but not as stable in the Mediterranean and Atlantic areas, where there is no heatwave occurrence over years.

2.4 Demographic Generalizability: Age-Specific Performance

As different ages of population may be affected by heatwaves in different ways, we demonstrate the performance of DEEPTHERM on different ages by three evaluation runs: 1) All ages, 2) Under-65 years of age, 3) 65+ years of age. Specifically, across these three runs, we use the same training and prediction pipeline as well as non-mortality data, but update the all-cause mortality data accordingly. Figure 4 shows the results for each age group stratified by type of heatwave and city.

Generally, on city-level predictions, the performance of DEEPTHERM in the 65+ and Under-65 population is similar to that of the entire population, except for the L2 heat waves, where DEEPTHERM yields a much higher recall in the Under-65 population (Figure 4a, 4b). For 65+ predictions, compared to the results on all-age, 65+ predictions yield higher precision in 9/12 cities with 12.6% average absolute difference to all-age (Figure 4e), and higher recall in 7/12 cities with 10.7% average absolute difference (Figure 4f). These lead to cumulatively 5.5% higher precision and 0.3% higher recall. For Under-65 predictions, 9 cities yield higher precision with 13.0% average absolute difference to all-age, and all cities yield higher recall with 16.7% average absolute difference. These lead to cumulatively 4.7% higher precision and 16.7% higher recall.

Same studies are also conducted in provincial predictions. To ensure enough heatwaves for each

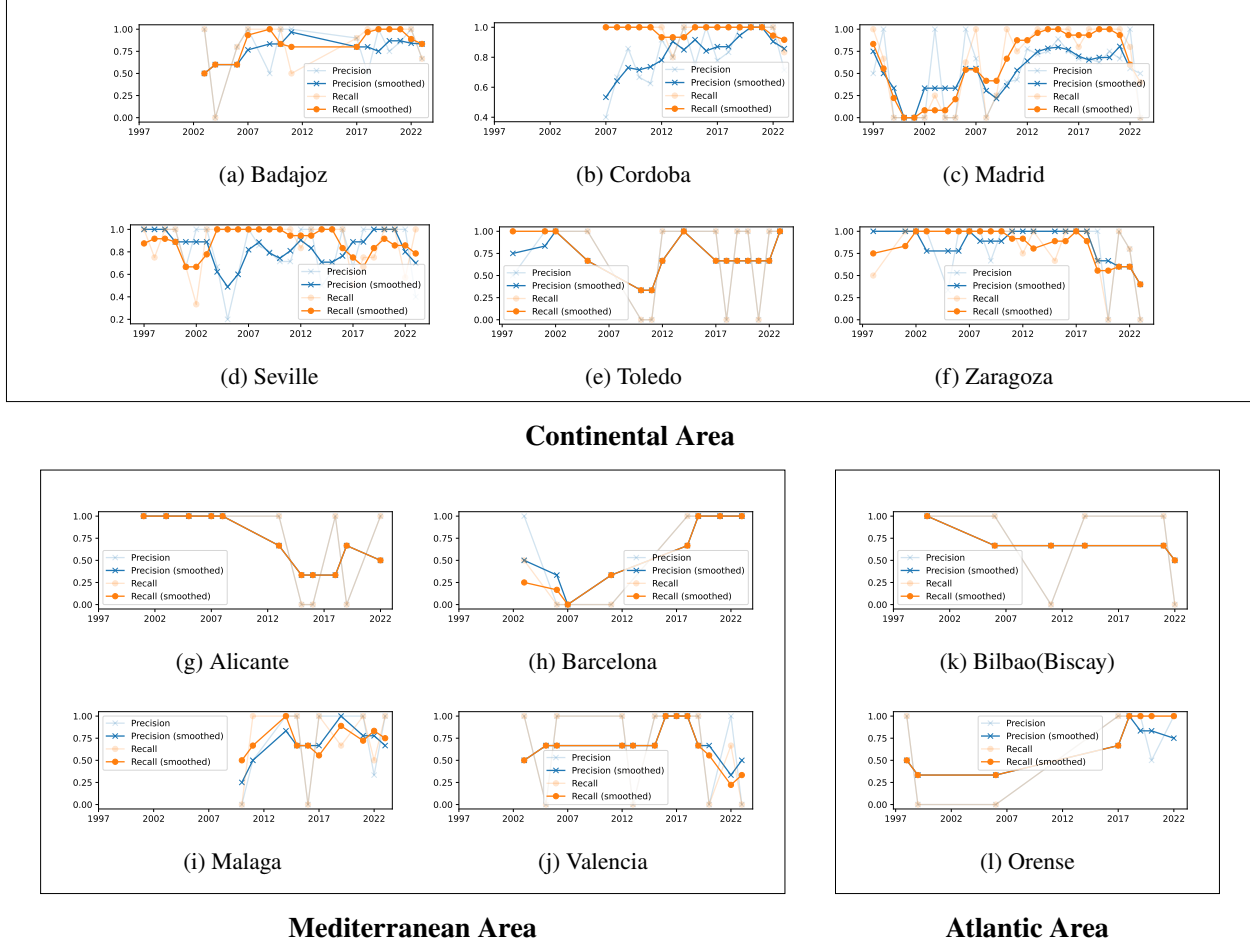


Figure 3: DEEPTHERM demonstrates consistent performance across most years, with improved accuracy as more data becomes available. The figures present annual heatwave prediction results (smoothed using a three-year sliding window) for city-level and provincial data from 1997 to 2023 across 12 selected Spanish cities, evaluated by Precision and Recall metrics. Cities are grouped by climate zone: 1) Continental, 2) Mediterranean, and 3) Atlantic. DEEPTHERM maintains stable performance across most years while showing gradual improvement over time, except during the COVID-19 pandemic period. Notably, despite the significant challenges of mortality prediction during the pandemic, DEEPTHERM achieves strong performance in recent years, particularly in Continental regions with more frequent heatwave occurrences. This suggests the model's particular effectiveness in areas with higher heatwave prevalence, highlighting its potential for broad impact in vulnerable regions.

population, we only study the 5 cities with most heatwaves. Generally, DEEPTHERM performs close on L1 heatwave predictions, but gets higher precision and recall in L2 heatwave predictions (Figure 4c, 4d). For 65+ predictions, compared with all-age results, DEEPTHERM receives higher precision in 2 cities with 5.8% mean absolute difference (Figure 4i), and higher recall in 3 cities with 3.4% mean absolute difference (Figure 4j). These lead to cumulatively 0.8% higher precision and 1.0% higher recall. For Under-65 predictions, DEEPTHERM receives higher precisions for 4 cities with 3.5% absolute difference, and higher recall for all cities with 7.0% absolute difference. This leads to cumulatively 1.5% higher precision and 7.0% higher recall.

2.5 Predictive Synthesis: Advantage of Utilizing Historical Mortality Data

One key advantage of DEEPTHERM, compared to previous deadly heatwave prediction approaches (21), is the capability of utilizing daily all-cause mortality history in the prediction. We examined such an advantage by comparing the predictive performance of DEEPTHERM with existing deadly heatwave models that leverage predictive accuracy yet are not capable of utilizing daily historical mortality (20, 21). Table 5 shows that model achieved significantly higher recall while maintaining superior precision, implying that DEEPTHERM, compared to baseline methods, significantly cuts off the number of missing alarms without causing more false alarms.

2.6 Adaptive Thresholding: Balancing False Alarms and Missed Detections

While prior predictions assume fixed threshold values in DEEPTHERM (aligned with the Level-1 and Level-2 heatwave definitions in Section 4.2), DEEPTHERM can adapt its thresholding strategy without retraining the model parameters. This allows the heat-related mortality predictions to be calibrated for higher (or lower) sensitivity, enabling adjustable alarm thresholds. To evaluate DEEPTHERM’s performance under different thresholding values, we vary the threshold from 0.01 to 0.50 in increments of 0.001 and plot the resulting false positive-to-false negative trade-off in Figure 6. For provincial classifications, the model exhibits sharp trade-offs between false negative and false positive rates across most thresholds, except within the ranges [0.2, 0.25] (L1) and [0.3, 0.35] (L2), which emerge as robust regimes for threshold selection. In contrast, city-level classifications show smoother trade-off curves, permitting greater flexibility in threshold choice. Alternative values may

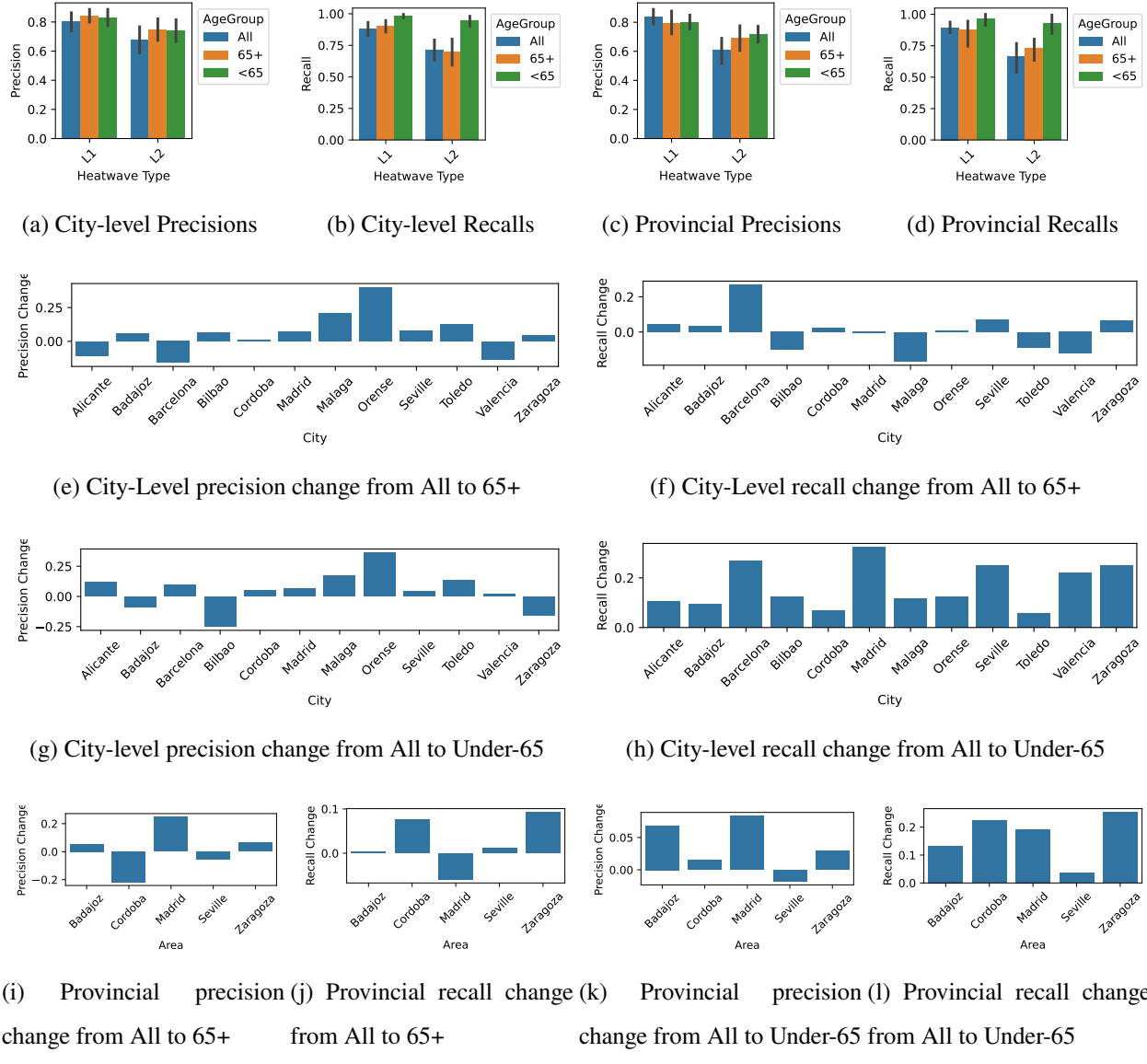
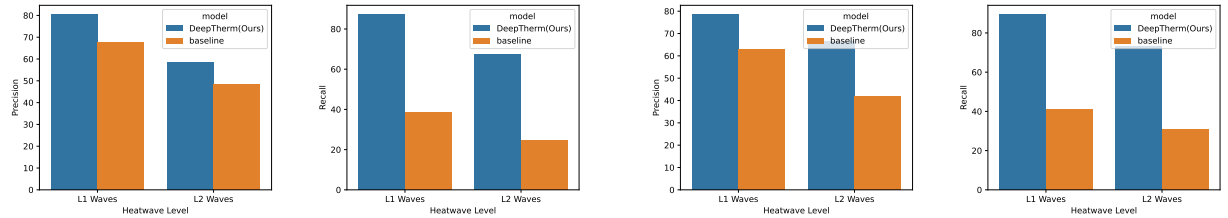


Figure 4: DEEPTherm demonstrates consistent performance across both younger (under 65) and older (65+) population groups in all cities. We evaluated DEEPTherm by replacing all-age mortality records with age-specific mortality data (Under-65 and 65+ populations). Figures (a)-(d) present the average precision and recall for both age groups across all cities and regions, while (e)-(l) display city-level and provincial variations in performance metrics (averaged across L1 and L2 heatwaves) compared to all-age population predictions. The results show that DEEPTherm maintains comparable performance when predicting heatwave impacts for both age groups relative to all-age predictions.



(a) Precision and Recall of provincial predictions against baseline models

(b) Precision and Recall of city-level predictions against baseline models

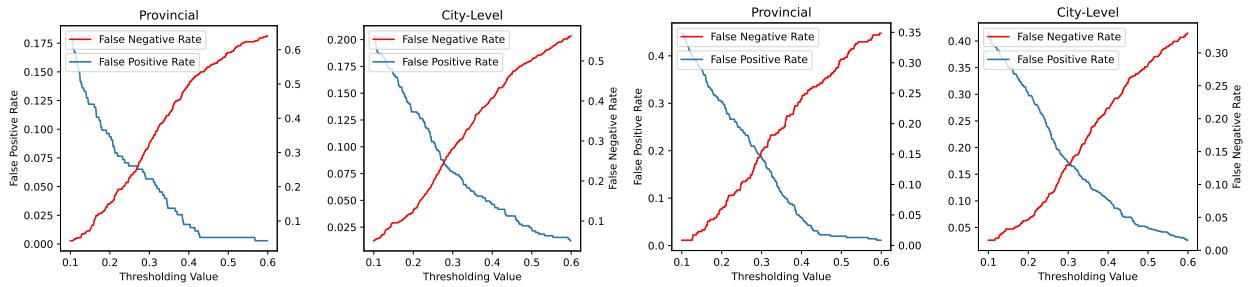
Figure 5: Comparing the prediction results of DEEPTHERM to previous deadly heatwave prediction methods that project non-mortality variables to excess mortality ratio and cannot use historical all-cause mortality records. DEEPTHERM achieves significantly better recall while maintaining superior precision, implying DEEPTHERM predicted more missing alarms without causing more false alarms. This highlights the advantage of capability inside using historical mortality data, which is introduced by our novelly designed dual-prediction pipeline.

also be selected if stricter constraints are imposed on either rate.

3 Discussion

Establishing early warning systems for deadly heatwaves is critical for mitigating heat-related health impacts and reducing excess mortality (40, 41), which is yet hard to achieve due to the difficulty in defining and estimating heat-related mortality records. Existing research primarily either remains on qualitative analyses of historical correlations between heat-related mortality and environmental indicators (42, 43, 44, 45), or is not capable of using the historical mortality information in the prediction of near-future excess heat-related mortality (20, 21). In contrast, DEEPTHERM provides a novel dual-line prediction pipeline, which enables operation using all-cause mortality records, significantly expanding its potential deployment to regions with high-quality surveillance data on daily mortality.

Our comprehensive evaluation across Spain demonstrates the model’s robust performance, indicating great potential in real-world scenarios. First, spatial evaluation shows that DEEPTHERM correctly identifies over 75% of L1 heatwaves and over half of L2 heatwaves correctly (Table 1a,



(a) False positive and false negative rates of L1 predictions
 under different decision thresholds
 (b) False positive and false negative rates of L2 predictions
 under different decision thresholds

Figure 6: DEEPTherm offers flexible threshold adjustment to balance false positives (false alarms) and false negatives (missed alarms) according to operational needs. The curves illustrate the trade-off between false positive and false negative rates across different threshold values, demonstrating how DEEPTherm can be adjusted to prioritize either alarm certainty or detection sensitivity. For provincial classifications, the ranges [0.2, 0.25] and [0.3, 0.35] serve as robust threshold regimes for L1 and L2, respectively, as they lie between two intervals of sharp fluctuations in both false positive and false negative rates, offering a stable balance. In contrast, city-level classification rates exhibit a smoother trend, allowing greater flexibility in threshold selection. While alternative values may be chosen under stricter constraints on either rate, these adjustments require no modifications to the underlying prediction modules (all-cause and baseline) and can be applied to any region. This adaptability enables policymakers to tailor DEEPTherm to diverse operational needs—whether minimizing false alarms or maximizing heatwave detection coverage.

1b), with the latter representing a particularly challenging prediction task due to their stricter excess mortality thresholds. Second, temporal evaluation of DEEPTherm reveals consistent performance across years(3), with only minor impacts from anomalous events like the COVID-19 pandemic. Third, DEEPTherm also successfully adapts to different age groups, accurately capturing variations in heatwave mortality patterns across demographics (4).

Notably, DEEPTherm achieved the aforementioned performance without requiring surveillance data that specifically identifies individual deaths as being "heat-related", relying instead only on all-cause mortality data. This is a significant advantage for real-world deployment, as determining which deaths are attributable to heat is complex and tends to underestimate the total burden of

heat on mortality. Specifically, counting deaths attributed as "heat-related" underestimates total excess deaths attributable to heat by about an order of magnitude (31, 46). We distinguish such an advantage by the superior performance of DEEPTHERM against baseline deadly heatwave prediction methods that are not capable of using daily all-cause mortality data as DEEPTHERM.

Furthermore, DEEPTHERM exhibits improved performance with more years of data as well as more heatwaves. For example, DEEPTHERM achieves higher accuracy in provinces and cities with more extensive heatwave records (Figure 1) and in more recent years (Figure 3). This positive correlation between data volume and model performance suggests DEEPTHERM is particularly well-suited for regions experiencing frequent heatwaves, where an effective early warning system could yield the most significant public health benefits by preventing heat-related mortality.

Another key strength of DEEPTHERM lies in its ability to effectively balance false alarms (i.e., false positives) and missed detections (i.e., false negatives) - a critical feature for real-world implementation. As heatwave alerts often directly inform policy decisions or activation of emergency or other community responses (47, 48), minimizing false alarms is essential to prevent unnecessary resource allocation while maintaining detection sensitivity. DEEPTHERM addresses this need through adjustable classification thresholds (Figure 6), enabling emergency managers to optimize the trade-off between false positive and false negative rates. Importantly, the model maintains a smooth balance between these error types, avoiding disproportionate decrease in either metric during threshold adjustment.

Still, the current implementation of DEEPTHERM faces several constraints. First, DEEPTHERM is currently designed to use real-time non-mortality and mortality data. Meanwhile, its effectiveness in regions with reporting delays—such as those serviced by the U.S. CDC, where mortality data may lag by months ((49))—remains uncertain. Additionally, DEEPTHERM's robustness to quality issues of collected data—such as missing or inaccurate temperature records—remains unverified. Furthermore, our validation has been conducted exclusively in Spain, where infrastructure and climate adaptation resources are relatively homogeneous across regions. Future research should evaluate DEEPTHERM 's performance in more diverse spatial contexts, particularly in areas with varying levels of heat resilience infrastructure, with ablations of various input availability.

4 Materials and Methods

4.1 Evaluation Data

We collected three forms of data that is required to evaluate DEEPTHERM: non-mortality data, all-cause mortality data, and synoptic weather-typing data.

Non-mortality Data is used as input for the all-cause mortality prediction. We collect daily meteorological data from Aemet Opendata¹ as our non-mortality data, which comes from stations that monitor weather at local airports, where available, else (Orense, Toledo) downtown weather stations. The collected data including four variables: temperature (Celsius), pressure (hPa), wind speed (m/s), and humidity (percentage).

All-cause Mortality Data is used in both all-cause and baseline mortality prediction. We collect 1) city-level daily mortality data from 1995 to 2023, released by Instituto Nacional de Estadística² (INE) 2) provincial daily mortality data from 2015 to 2023, collected by MoMo³. Specifically, INE data is a private dataset where our data was obtained upon request; MoMo is a publicly available dataset, where we get the data through the public panel.

Synoptic Weather-typing Data is used to predict the occurrences of heatwaves in near-future. We collect the data from the online panel of Spatial Synoptic Classification v3.0⁴, which contains the SSC codes for most of the main cities worldwide.

We collected data from twelve provinces and their corresponding homonymous capital cities, except Biscay (province), whose capital city is Bilbao. During the selection of cities and provinces, population was a major criterion. The final set includes nine of the twelve most populated cities in Spain, including the top six. We also considered a variety of climatic scenarios as shown in Figure 2. Specifically, we balanced coast cities (4), interior cities (6), and interior cities close to the mouth of a river (2, Seville and Bilbao). The provincial set includes the six most populous provinces in Spain, accounting for some 45% of the population of the country. Seven provinces are landlocked. Orense is a low-populated, landlocked province in Galicia (Northwestern Spain, Atlantic region). However, the city of Orense has a hot summer Mediterranean climate (Csb, in the

¹https://www.aemet.es/en/datos_abiertos/AEMET_OpenData

²<https://www.ine.es/en/>

³https://momo.isciii.es/panel_momo/

⁴<https://sheridan.geog.kent.edu/ssc3.html>

	Alicante	Badajoz	Barcelona	Bilbao(Biscay)	Cordoba	Madrid	Malaga	Orense	Seville	Toledo	Valencia	Zaragoza
Provincial Population(k)	1993	666	5878	1159	774	7009	1775	305	1969	743	2711	988
City-level Population(k)	335	148	1620	346	326	3256	578	105	684	84	792	675
Climate (city)	Bsh	Csa	Csa	Cfb	Csa	Bsk/Csa	Csa	Csb	Csa	Bsk	Bsh	Bsk

(a) Population and Climate Overview

		Alicante	Badajoz	Barcelona	Bilbao	Cordoba	Madrid	Malaga	Orense	Seville	Toledo	Valencia	Zaragoza	Total
MoMo (Provincial)	All	3	49	4	2	53	50	13	6	36	11	9	19	255
	L1	1	40	3	1	39	32	8	5	26	10	6	14	185
	L2	0	26	1	1	25	14	1	4	19	4	4	11	110
INE (city-level)	All	14	69	9	6	124	166	21	10	132	25	18	55	649
	L1	11	57	7	4	97	98	13	7	97	22	14	44	471
	L2	9	53	4	4	77	34	7	4	62	15	7	32	308

(b) Heatwave Statics

Table 2: Our selected cities and provinces cover a variety of population size as well as heatwave appearance frequency. Table (a) shows the population sizes of the selected cities in our dataset and their located provinces, as well as their climate conditions. Population numbers were retrieved from the Eurostat population by NUTS3 (Nomenclature of Territorial Units for Statistics level 3 available at https://doi.org/10.2908/DEMO_R_PJANGRP3) (province) and geonames database (<https://geonames.org>) (city). Codes are provided in Supplementary. Table (b) shows the count of heatwaves in each city (province) across all the collected time periods. Climate Köppen-Geiger codes for the period 1991-2020 were retrieved from Figure 5 in Ref. 50.

Köppen-Geiger climate classification) associated with the orography and served as a test for our model’s performance in such conditions. An overview of the population sizes and appearance of the heatwaves of each city and the corresponding province is shown in Figure 2, where the population data are collected from the NUTS3 provincial population database and Geonames city population database.

4.2 Problem Setup

We formulate the deadly heatwave prediction problem correspondingly: for a certain day t , we have the historical all-cause mortality data $X_{:t}$, the historical non-mortality data $Z_{:t}$, and the synoptic weather-typing data extended to h -day future $N_{:t+h}$. If $N_{:t+h}$ shows there is a heatwave between day t and $t + h$, we run DEEPTHERM to predict 1) whether the heatwave will be deadly or not, 2) whether the heatwave will be extreme or not. This will then involve two settings: 1) definition of heatwaves, 2) definition of deadly and L2 heatwaves

Definition of Heatwaves Following prior work in synoptic classification (36, 37), we employ the Spatial Synoptic Classification (SSC) pipeline to identify heatwave events. Specifically, each day is categorized into one of six types: Dry Polar (DP), Dry Moderate (DM), Dry Tropical (DT), Moist Polar (MP), Moist Moderate (MM), or Moist Tropical (MT). A heatwave is defined as a sequence of consecutive days where, for each day in the sequence, at least one of the following conditions holds over a three-day sliding window: 1) all three days are Dry Tropical days, or 2) the three-day window contains both Dry Tropical and Moist Tropical days.

Definition of Heatwave Levels To test the performance of DEEPTHERM under broader or stricter heatwave standards, we categorize heatwaves into three levels: 0, 1, 2, according to the ratio of how much the heat-related mortality exceeds baseline mortality during the heatwave. Specifically, for a heatwave spanning N days, we compute such a ratio R by:

$$R = \max_{t \in N} \left(\frac{X_t - \tilde{X}_t}{\tilde{X}_t} \right), \quad (1)$$

where \tilde{X}_t and X_t are baseline mortality and all-cause mortality of day t , respectively. While X_t directly comes from data, \tilde{X}_t is generated by a Quasi-Poisson regression model (51). We establish such a Quasi-Poisson model in the same way as the baseline prediction module of DEEPTHERM, which will be described in detail in Section 4.3.2. For a heatwave, if the ratio R goes beyond 15%, we mark the heatwave as a level 1 (L1) heatwave. And if the ratio goes beyond 30%, we further mark the heatwave as a level 2 (L2) heatwave. By this definition, L2 heatwaves are also classified as deadly. An overview of deadly and L2 heatwave distributions across cities and provinces is provided in Table 2b.

4.3 Design of DEEPTHERM

DEEPTHERM is composed of three components: 1) all-cause mortality prediction module 2) baseline mortality prediction module 3) decision module.

4.3.1 All-cause Mortality Prediction Module

The all-cause mortality prediction module is established on a deep-learning-based predictor, named Transformer (52), which produces sequence-to-sequence predictions based on the self-attention mechanism. Specifically, note the input mortality history as $X \in \mathbb{R}^{1 \times T}$ where T is the length of mortality history, and the non-mortality history as $Z \in \mathbb{R}^{m \times T}$ where m is the number of collected non-mortality variables. The input to the model will then be $X' = \{X; Z\} \in \mathbb{R}^{(m+1) \times T}$. Transformer will first produce three matrices named query Q , key K , and value V depending on learnable weights $W_K, W_Q, W_V \in \mathbb{R}^{(m+1) \times d_K}$, which will be calculated towards a self-attention output:

$$Q = (X')^T W_Q, \quad (2)$$

$$K = (X')^T W_K, \quad (3)$$

$$V = (X')^T W_V, \quad (4)$$

$$Z' = \text{softmax} \left(\frac{QK^T}{\sqrt{d_K}} \right) V. \quad (5)$$

Such a procedure will happen iteratively through every layer, that is, the input X' in each layer corresponds to the output Z' from the previous layer. After the final layer, the output prediction \tilde{X} will be produced by a linear projection f_p based on the output from the last layer: $\tilde{X} = f_p(Z')$.

In our evaluations, we set $T = 14$, inputting the 14-day history of both observed mortality and non-mortality factors to the model, and prompt the model to predict total mortality up to 5 days in the future. All the input factors are linearly normalized regarding the historical max and min values:

$$\hat{X}_t = \frac{X_t - \min_{j \in [1:t]} X_j}{\max_{j \in [1:t]} X_j - \min_{j \in [1:t]} X_j}. \quad (6)$$

We train the model by minimizing the mean squared error (MSE) between the prediction and the ground truth mortality. Such training is done in a *real-time* manner. Specifically, when predicting the mortality for year Y , we assume the model is accessible to all mortality data up to year $Y - 1$.

Given that our data is collected from 1995 to 2023, we simulated the prediction procedure each year from 1997 to 2023, updating the model of each year based on the trained model from the previous year. Details of training and model hyperparameters can be found in Supplementary.

4.3.2 Baseline Mortality Prediction Module

Following the approach outlined in a previous study (51), we estimate future baseline mortality using a Quasi-Poisson regression model. Specifically, we fit the model to historical all-cause mortality data, incorporating selected covariates that account for temporal trends, such as day-of-the-week and holiday indicators. We then apply the fitted model to the covariates from the prediction horizon to generate corresponding mortality estimates. Since the inputs to the Quasi-Poisson model exclude heat-related variables, this modeling process effectively acts as a denoising procedure, disentangling heat-related mortality from all-cause mortality. Thus, the resulting predictions can be interpreted as approximations of baseline mortality, independent of heat-related influences. Empirically, when training this baseline mortality predictor, we restrict the training data to all-cause mortality records from the past two years. This constraint is necessary because baseline mortality may exhibit distributional shifts over longer time periods due to population changes.

4.3.3 Decision Module

Given the predicted all-cause mortality and baseline mortality in the future, the decision module determines whether to raise an alarm for a heatwave based on weather-typing data. Specifically, for a heatwave period $T = [i, i + h]$ spanning days i to day $i + h$, let $X_{all-cause}(t)$ (where $t \in [i, i + h]$) denote the predicted all-cause mortality for day t , and $X_{non-hr}(t)$ represent the predicted baseline mortality. The decision module first calculates the heat-related mortality by subtracting baseline mortality from all-cause mortality:

$$X_{hr}(t) = X_{all-cause}(t) - X_{non-hr}(t), \forall t \in T \quad (7)$$

Next, it computes the relative excess of heat-related mortality over baseline mortality for each

day:

$$R(t) = \frac{X_{hr}}{X_{non-hr}} = \frac{X_{all-cause}(t) - X_{non-hr}(t)}{X_{non-hr}(t)}, \forall t \in T \quad (8)$$

If any $R(t)$ exceeds a predefined threshold α , an alarm is triggered for the heatwave. Without changing the predictions of $X_{all-cause}$ and X_{non-hr} , we can balance the alarms of heatwaves by flexibly adjusting α , which is investigated in Section 2.6.

4.4 Baseline Deadly Heatwave Prediction Models

One key advantage of DEEPTHERM is the capability of using all-cause mortality history, which is not yet achieved by existing deadly heatwave prediction methods. We hereby introduce two baselines from the previous deadly heatwave prediction methods: (20) performs a linear projection from seasonal splines of time and temperatures to excess mortality. (21) performs an exponential projection from daily temperature and annual average mortality to excess mortality. We maintained their calculation of the excess mortality ratio. Furthermore, we allowed a calibration in model parameters as well as decision threshold upon the same training data as DEEPTHERM for a fair comparison.

References and Notes

1. J. Kysely, Recent severe heat waves in central Europe: how to view them in a long-term prospect? *International Journal of Climatology: A Journal of the Royal Meteorological Society* **30** (1), 89–109 (2010).
2. A. B. Pezza, P. Van Rensch, W. Cai, Severe heat waves in Southern Australia: synoptic climatology and large scale connections. *Climate Dynamics* **38**, 209–224 (2012).
3. K. K. Murari, S. Ghosh, A. Patwardhan, E. Daly, K. Salvi, Intensification of future severe heat waves in India and their effect on heat stress and mortality. *Regional Environmental Change* **15** (4), 569–579 (2015).
4. J.-M. Robine, *et al.*, Death toll exceeded 70,000 in Europe during the summer of 2003. *Comptes Rendus. Biologies* **331** (2), 171–178 (2008).
5. D. Barriopedro, E. M. Fischer, J. Luterbacher, R. M. Trigo, R. García-Herrera, The hot summer of 2010: redrawing the temperature record map of Europe. *Science* **332** (6026), 220–224 (2011).
6. A. Gasparrini, B. Armstrong, The impact of heat waves on mortality. *Epidemiology* **22** (1), 68–73 (2011).
7. J. Ballester, *et al.*, Heat-related mortality in Europe during the summer of 2022. *Nature medicine* **29** (7), 1857–1866 (2023).
8. R. García-Herrera, J. Díaz, R. M. Trigo, J. Luterbacher, E. M. Fischer, A review of the European summer heat wave of 2003. *Critical Reviews in Environmental Science and Technology* **40** (4), 267–306 (2010).
9. J. Garssen, C. Harmsen, J. d. Beer, The effect of the summer 2003 heat wave on mortality in the Netherlands. *Eurosurveillance* **10** (7-9), 165–167 (2005).
10. F. Simón, G. Lopez-Abente, E. Ballester, F. Martínez, Mortality in Spain during the heat waves of summer 2003. *Euro surveillance: bulletin européen sur les maladies transmissibles= European communicable disease bulletin* **10** (7), 9–10 (2005).

11. C. Brimicombe, *et al.*, Preventing heat-related deaths: the urgent need for a global early warning system for heat. *PLoS Climate* **3** (7), e0000437 (2024).
12. S. Chattopadhyay, D. Jhajharia, G. Chattopadhyay, Univariate modelling of monthly maximum temperature time series over northeast India: neural network versus Yule–Walker equation based approach. *Meteorological Applications* **18** (1), 70–82 (2011).
13. K. Abhishek, M. P. Singh, S. Ghosh, A. Anand, Weather forecasting model using artificial neural network. *Procedia Technology* **4**, 311–318 (2012).
14. K. A. McKinnon, A. Rhines, M. Tingley, P. Huybers, Long-lead predictions of eastern United States hot days from Pacific sea surface temperatures. *Nature Geoscience* **9** (5), 389–394 (2016).
15. C. Prodhomme, *et al.*, Seasonal prediction of European summer heatwaves. *Climate Dynamics* pp. 1–18 (2022).
16. A. Gasparrini, *et al.*, Mortality risk attributable to high and low ambient temperature: a multicountry observational study. *The lancet* **386** (9991), 369–375 (2015).
17. S. Kang, E. A. Eltahir, North China Plain threatened by deadly heatwaves due to climate change and irrigation. *Nature communications* **9** (1), 2894 (2018).
18. A. M. Vicedo-Cabrera, *et al.*, The burden of heat-related mortality attributable to recent human-induced climate change. *Nature climate change* **11** (6), 492–500 (2021).
19. M. KA, U. ZL, The deadly impact of urban heat. *Nature* **595**, 349 (2021).
20. R. W. Mathes, K. Ito, K. Lane, T. D. Matte, Real-time surveillance of heat-related morbidity: Relation to excess mortality associated with extreme heat. *PLoS One* **12** (9), e0184364 (2017).
21. M. N. Mistry, A. Gasparrini, Real-time forecast of temperature-related excess mortality at small-area level: towards an operational framework. *Environmental Research: Health* **2** (3), 035011 (2024).

22. D. A. Stainforth, M. R. Allen, E. R. Tredger, L. A. Smith, Confidence, uncertainty and decision-support relevance in climate predictions. *Philosophical Transactions of the Royal Society A: Mathematical, Physical and Engineering Sciences* **365** (1857), 2145–2161 (2007).
23. J. T. Ripberger, *et al.*, False alarms and missed events: The impact and origins of perceived inaccuracy in tornado warning systems. *Risk analysis* **35** (1), 44–56 (2015).
24. J. LeClerc, S. Joslyn, The cry wolf effect and weather-related decision making. *Risk analysis* **35** (3), 385–395 (2015).
25. J. N. Burgeno, S. L. Joslyn, The impact of weather forecast inconsistency on user trust. *Weather, climate, and society* **12** (4), 679–694 (2020).
26. S. C. Sheridan, T. J. Dolney, Heat, mortality, and level of urbanization: measuring vulnerability across Ohio, USA. *Climate research* **24** (3), 255–265 (2003).
27. M. Park, D. Jung, S. Lee, S. Park, Heatwave damage prediction using random forest model in Korea. *Applied sciences* **10** (22), 8237 (2020).
28. D. M. Hondula, S. Meltzer, R. C. Balling Jr, P. Iñiguez, Spatial analysis of United States National Weather Service excessive heat warnings and heat advisories. *Bulletin of the American Meteorological Society* **103** (9), E2017–E2031 (2022).
29. P. Li, Y. Yu, D. Huang, Z.-H. Wang, A. Sharma, Regional heatwave prediction using graph neural network and weather station data. *Geophysical Research Letters* **50** (7), e2023GL103405 (2023).
30. J. M. Martin-Olalla, *et al.*, From heat wave Zoe to heat wave Vera: a two-year ex post evaluation of the categorization and naming heat wave system ProMeteo in Seville, Spain. *Zenodo* (2024), doi:10.5281/zenodo.12821713.
31. K. R. Weinberger, D. Harris, K. R. Spangler, A. Zanobetti, G. A. Wellenius, Estimating the number of excess deaths attributable to heat in 297 United States counties. *Environmental Epidemiology* **4** (3), e096 (2020).

32. Y. E. Lo, D. M. Mitchell, R. Thompson, E. O'Connell, A. Gasparrini, Estimating heat-related mortality in near real time for national heatwave plans. *Environmental research letters* **17** (2), 024017 (2022).

33. H. Wu, *et al.*, Timesnet: Temporal 2d-variation modeling for general time series analysis. *arXiv preprint arXiv:2210.02186* (2022).

34. S. Y. Kim, *et al.*, A deep learning model for real-time mortality prediction in critically ill children. *Critical care* **23** (1), 279 (2019).

35. S. Ventura, J. R. Miró, J. C. Peña, G. Villalba, Analysis of synoptic weather patterns of heatwave events. *Climate Dynamics* **61** (9), 4679–4702 (2023).

36. S. C. Sheridan, The redevelopment of a weather-type classification scheme for North America. *International Journal of Climatology: A Journal of the Royal Meteorological Society* **22** (1), 51–68 (2002).

37. D. M. Hondula, J. K. Vanos, S. N. Gosling, The SSC: a decade of climate–health research and future directions. *International journal of biometeorology* **58**, 109–120 (2014).

38. C. S. Cheng, G. Li, Q. Li, H. Auld, A synoptic weather-typing approach to project future daily rainfall and extremes at local scale in Ontario, Canada. *Journal of Climate* **24** (14), 3667–3685 (2011).

39. C. Siegert, D. Leathers, D. Levia, Synoptic typing: Interdisciplinary application methods with three practical hydroclimatological examples. *Theoretical and Applied Climatology* **128**, 603–621 (2017).

40. P. Michelozzi, *et al.*, Surveillance of summer mortality and preparedness to reduce the health impact of heat waves in Italy. *International journal of environmental research and public health* **7** (5), 2256–2273 (2010).

41. J. J. Hess, *et al.*, Public health preparedness for extreme heat events. *Annual Review of Public Health* **44** (1), 301–321 (2023).

42. L. S. Kalkstein, J. S. Greene, An evaluation of climate/mortality relationships in large US cities and the possible impacts of a climate change. *Environmental health perspectives* **105** (1), 84–93 (1997).

43. J. Tan, *et al.*, Heat wave impacts on mortality in Shanghai, 1998 and 2003. *International journal of biometeorology* **51**, 193–200 (2007).

44. L. Liang, L. Yu, Z. Wang, Identifying the dominant impact factors and their contributions to heatwave events over mainland China. *Science of the Total Environment* **848**, 157527 (2022).

45. L. S. Kalkstein, D. P. Eisenman, E. B. de Guzman, D. J. Sailor, Increasing trees and high-albedo surfaces decreases heat impacts and mortality in Los Angeles, CA. *International journal of biometeorology* **66** (5), 911–925 (2022).

46. D. Shindell, *et al.*, The effects of heat exposure on human mortality throughout the United States. *GeoHealth* **4** (4), e2019GH000234 (2020).

47. D. Lowe, K. L. Ebi, B. Forsberg, Heatwave early warning systems and adaptation advice to reduce human health consequences of heatwaves. *International journal of environmental research and public health* **8** (12), 4623–4648 (2011).

48. J. Kravchenko, A. P. Abernethy, M. Fawzy, H. K. Lyerly, Minimization of heatwave morbidity and mortality. *American journal of preventive medicine* **44** (3), 274–282 (2013).

49. F. Ahmad, J. Cisewski, D. Hoyert, Maternal mortality rates in the United States, 2025. *NCHS Health E Stats [Internet]* (2025).

50. A. Chazarra-Bernabé, B. Lorenzo-Mariño, R. Romero-Fresneda, J. Moreno-García, *Evolución de los climas de Köppen en España en el periodo 1951-2020*, Tech. rep., Agencia Estatal de Meteorología (2022), doi:10.31978/666-22-011-4.

51. Z. Lin, *et al.*, Daily heat and mortality among people experiencing homelessness in 2 urban US counties, 2015-2022. *American journal of epidemiology* **193** (11), 1576–1582 (2024).

52. A. Vaswani, *et al.*, Attention is all you need. *Advances in neural information processing systems* **30** (2017).

53. A. Paszke, Pytorch: An imperative style, high-performance deep learning library. *arXiv preprint arXiv:1912.01703* (2019).
54. F. Pedregosa, *et al.*, Scikit-learn: Machine Learning in Python. *Journal of Machine Learning Research* **12**, 2825–2830 (2011).

Author contributions: S.X., Z.Z., J.M.M.-O., A.R., G.A.W., B.A.P. conceived the experiments, S.X., Z.Z., M.S. conducted the experiments, S.X., Z.Z., J.M.M.-O., A.R., G.A.W., B.A.P. analyzed the results, S.X., Z.Z., J.M.M.-O., A.R., G.A.W., B.A.P. reviewed the manuscript.

Competing interests: There are no competing interests to declare.

Data and materials availability: Our codes are available in <https://github.com/SigmaTsing/DeepTherm>. The used mortality and non-mortality data should be acquired upon proper request to MoMo, INE database, Aemet Opendata, and Spatial Synoptic Classification V3.0, respectively.

Supplementary materials

Supplementary Text

Tables S1 to S4

Figure S1

Supplementary Materials for Modular Deep-Learning-Based Early Warning System for Deadly Heatwave Prediction

Shangqing Xu^{1*}, Zhiyuan Zhao¹, Megha Sharma¹, José María Martín-Olalla²,
Alexander Rodríguez³, Gregory A. Wellenius⁴, B. Aditya Prakash^{1*}

*Corresponding authors. Email: sxu452@gatech.edu, badityap@cc.gatech.edu

This PDF file includes:

Supplementary Text

Tables S1 to S4

Figure S1

Supplementary Information

Data Collection

We show the details of the collected data here.

Mortality Data

City-Level

We collect city-level mortality data through requests to INE database ⁵, maintained by Instituto Nacional de Estadística (National Statistics Institute) of Spain. The collected data contains daily all-cause mortality records of Hombre (Men) and Mujer (Women) that is aggregated within 5-year bins of age. We aggregate the mortality through both genders.

Provincial

We collect provincial mortality data through the public panel of MoMo ⁶, maintained by National Institute of Health Carlos III (ISCIII). The collected data contains daily all-cause mortality records aggregated into eight age bins: “all”, “0-14”, “15-44”, “45-64”, “65-74”, “75-84”, “+65”, and “+85”. We use the *defunciones_observadas* column in data as the daily mortality, aggregating between age bins according to corresponding settings.

Non-mortality Data

We collect daily non-mortality data from the Aemet Opendata ⁷, maintained by Ministerio para la Transición Ecológica y el Reto Demográfico (Ministry for the Ecological Transition and the Demographic Challenge) of Spain. The collected data contains daily averages of temperature (Celsius), pressure (hPa), wind speed(m/s), and humidity (percentage) of near-land air, starting from 1970.

⁵<https://www.ine.es/en/>

⁶https://momo.isciii.es/panel_momo/

⁷https://www.aemet.es/en/datos_abiertos/AEMET_OpenData

Synoptic Weather-typing Data

We collect synoptic weather-typing data from the public panel of Spatial Synoptic Classification V3.0⁸. The collected data contains daily synoptic weather prototypes, starting from 1970s or 1980s. Instead of obtaining the original synoptic codes in our input data, we preprocess them into boolean heatwave indicators according to the definition described in Section 4.2.

Evaluation Metrics

We evaluate DEEPTHERM under a binary classification setting: heatwaves which are labeled as deadly (extreme) or safe, and DEEPTHERM predicts if these heatwaves are deadly (extreme) or safe. The predictions from DEEPTHERM are then evaluated into one of the four classes:

- 1 True Positive (TP), where DEEPTHERM correctly recognize a deadly (extreme) heatwave
- 2 False Positive (FP), where DEEPTHERM wrongly categorize a safe heatwave as a deadly (extreme) heatwave. The occurrence of FP will lead to a false alarm
- 3 False Negative (FN), where DEEPTHERM wrongly categorize a deadly (extreme) heatwave as a safe heatwave
- 4 True Negative (TN), where DEEPTHERM correctly recognize a safe heatwave

Given the counted number of these four classes, we calculate the evaluation metrics correspondingly:

$$\text{Accuracy} = \frac{\text{TP} + \text{TN}}{\text{TP} + \text{TN} + \text{FP} + \text{FN}} \quad (\text{S1})$$

$$\text{Precision} = \frac{\text{TP}}{\text{TP} + \text{FP}} \quad (\text{S2})$$

$$\text{Recall} = \frac{\text{TP}}{\text{TP} + \text{FN}} \quad (\text{S3})$$

$$\text{F1} = \frac{\text{Recall} \times \text{Precision}}{\text{Recall} + \text{Precision}} \quad (\text{S4})$$

⁸<https://sheridan.geog.kent.edu/ssc3.html>

Codes for NUTS and Geonames Dataset

We show the codes for NUTS and Geonames dataset corresponded to each city and province, which we used to get the statics in Table 2.

	Alicante	Badajoz	Barcelona	Bilbao(Biscay)	Cordoba	Madrid	Malaga	Orense	Seville	Toledo	Valencia	Zaragoza
NUTS3 code	ES521	ES431	ES511	ES213	ES613	ES300	ES617	ES113	ES618	ES425	ES523	ES243
Geonames ID	2521978	2519240	3128760	3128026	2519240	3117735	2514256	3114965	2510911	2510409	2509954	3104324

Table S1: NUTS3 and ID geonames codes for each province (NUTS3) and city (ID).

Implementation Details

We describe details of 1) how we preprocess the input data before feeding them into DEEPTherm 2) how we implement the mortality predictors and train them during the evaluations.

Data Preprocessing

Normalization For mortality data, we retain the original values in city-level datasets, while provincial-level mortality data are normalized by dividing by one hundred. For meteorological data, each dimension is independently normalized using the historical maximum and mean values from all available data.

Missing Data

For days with missing mortality data (which only occurs in early 2020 and thus does not interfere with deadly heatwave prediction evaluation), we impute them using the mean value of the corresponding month (calculated from all previous years). For missing meteorological data, we fill gaps with the mean value of all preceding days in the dataset.

Synoptic Codes of Heatwave Occurrence

To streamline the evaluation of DEEPTherm, we reuse pre-generated synoptic codes obtained from the official Spatial Synoptic Classification website⁹. Since these codes are derived from

⁹<https://sheridan.geog.kent.edu/ssc3.html>

corresponding meteorological data, their use does not introduce additional data requirements beyond those already available to DEEPTherm, ensuring no risk of data requirement violations.

Mortality Predictors

Transformer

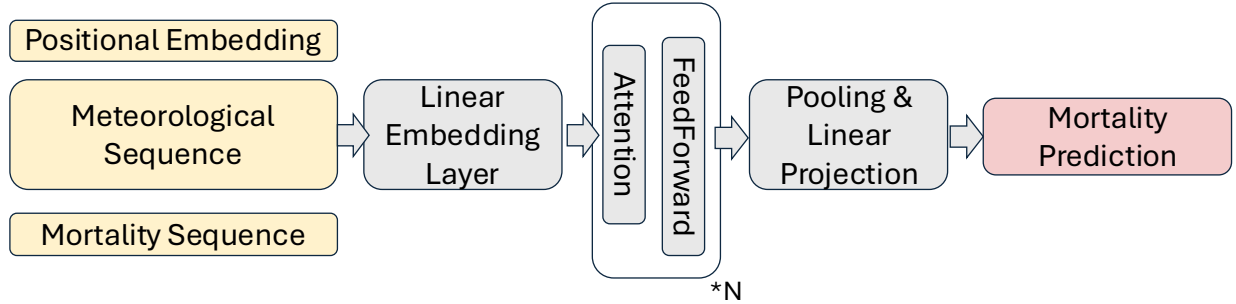


Figure S1: Overview of the structure of Transformer model, which is used to predict all-cause mortality.

As illustrated in Figure S1, we employ an attention-based deep learning model, Transformer, as our all-cause mortality predictor. The model first concatenates input mortality and meteorological sequences with positional embeddings, forming a multivariate sequence where each dimension corresponds to an original feature from mortality data, meteorological data, or positional embeddings. This sequence is then projected into an embedding space via a linear transformation. The embedded input is processed recursively through an attention module to produce an output embedding sequence. Finally, the output embeddings are pooled and projected to generate the final mortality prediction. All implementations are executed using PyTorch (53).

For positional embeddings, we use a two-dimensional sequence composed of sine and cosine waves. The attention layers are configured with an embedding dimension of 32, 2 attention blocks (each with 2 attention heads), and a 2-layer MLP (hidden dimension: 32) for the final projection. In the first year of training, the model is trained for 300 epochs with a learning rate of 10^{-4} learning rate. For subsequent years, the model is initialized with weights from the previous year and fine-tuned for another 300 epochs at the same learning rate.

Baseline Mortality Predictor

We use a quasi-Poisson model as our baseline mortality predictor. The predictor incorporates three input variables: 1) Day of the week (encoded as integers, where 1 = Monday and 7 = Sunday), 2) Day of the year (ranging from 0 for the first day to 364 or 365 for the last day), 3) Holiday indicator (binary, with 1 denoting an official Spanish holiday and 0 otherwise). Given these variables, we prompt the quasi-Poisson model to fit the all-cause mortality data in two years. Every time the model gets re-trained, the parameters of the predictor will be calibrated from scratch.

Baseline Models

XGBoost We use the implementation of XGBoost in their official python package ¹⁰. Specifically, we use the *XGBoostRegressor*, setting the number of estimators as 1000, learning rate as 0.01, max depth as 6, subsample rate as 0.8, column sample by tree as 0.8, and early stopping rounds as 50. We optimize the model towards minimizing squared error, and format the input data in the same way as DEEPTHERM.

Random Forest We use the implementation of random forest from scikit-learn (54), set the number of estimators as 1000, and keep all other parameters as default. The input is formatted in the same way as DEEPTHERM.

Original Result Tables

We show here the original experiment results of each city, each heatwave level, each population, for city-level and provincial classifications. Original prediction logs can be accessed in our Github repo. Table S2 shows the results of all-age classifications, Table S3 shows the results of 65+ classifications, and Table S4 shows the results of under-65 classifications.

¹⁰https://xgboost.readthedocs.io/en/release_3.0.0/

	Provincial								City-Level							
	Level 1				Level 2				Level 1				Level 2			
City	TP	FP	FN	TN	TP	FP	FN	TN	TP	FP	FN	TN	TP	FP	FN	TN
Alicante	1	0	0	2	0	0	0	3	9	1	2	2	8	2	1	3
Badajoz	39	5	1	4	19	14	7	9	52	11	5	1	44	10	9	6
Barcelona	2	1	1	0	0	1	1	2	5	0	2	2	2	1	2	4
Biscay	1	1	0	0	0	0	1	1	4	2	0	0	3	0	1	2
Cordoba	34	3	5	11	17	6	8	22	95	20	2	7	64	28	13	19
Madrid	27	5	5	13	6	8	8	28	85	40	13	28	22	24	12	104
Malaga	6	1	2	4	1	3	0	9	11	6	2	2	5	5	2	9
Orense	5	1	0	0	3	1	1	1	7	3	0	0	3	5	1	1
Sevilla	24	6	2	4	16	8	3	9	85	23	12	12	37	23	25	47
Toledo	7	0	3	1	3	5	1	2	19	3	3	0	14	7	1	3
Valencia	6	1	0	2	2	3	2	2	13	1	1	3	4	1	3	10
Zaragoza	12	4	2	1	7	4	4	4	37	4	7	7	19	7	13	16

Table S2: The original results of all-age classifications

	Provincial								City-Level							
	Level 1				Level 2				Level 1				Level 2			
City	TP	FP	FN	TN	TP	FP	FN	TN	TP	FP	FN	TN	TP	FP	FN	TN
Alicante	-	-	-	-	-	-	-	-	10	3	0	1	7	4	1	2
Badajoz	35	7	3	4	23	8	6	12	58	6	3	2	51	9	5	4
Barcelona	-	-	-	-	-	-	-	-	6	2	0	1	3	2	1	3
Bilbao(Biscay)	-	-	-	-	-	-	-	-	4	1	1	0	3	0	1	2
Cordoba	34	15	2	2	19	17	6	11	100	18	3	3	72	30	9	13
Madrid	20	1	12	17	9	2	8	31	82	33	23	28	27	20	27	92
Malaga	-	-	-	-	-	-	-	-	13	3	4	1	6	2	7	6
Orense	-	-	-	-	-	-	-	-	8	0	1	1	7	1	1	1
Sevilla	21	8	1	6	10	6	2	18	98	14	6	14	52	24	25	31
Toledo	-	-	-	-	-	-	-	-	22	1	1	1	14	3	7	1
Valencia	-	-	-	-	-	-	-	-	12	2	1	3	3	2	6	7
Zaragoza	13	4	1	1	9	3	3	4	40	7	6	2	28	4	12	11

Table S3: The original results of 65+ classifications

	Provincial								City-Level							
	Level 1				Level 2				Level 1				Level 2			
City	TP	FP	FN	TN	TP	FP	FN	TN	TP	FP	FN	TN	TP	FP	FN	TN
Alicante	-	-	-	-	-	-	-	-	13	1	0	0	13	1	0	0
Badajoz	41	7	0	1	35	12	1	1	50	18	0	1	48	18	1	2
Barcelona	-	-	-	-	-	-	-	-	9	0	0	0	6	1	2	0
Bilbao(Biscay)	-	-	-	-	-	-	-	-	4	2	0	0	3	3	0	0
Cordoba	45	7	0	1	42	9	0	2	102	17	1	4	87	26	4	7
Madrid	32	10	5	3	19	9	5	17	116	40	2	8	74	63	4	25
Malaga	-	-	-	-	-	-	-	-	14	4	1	2	12	5	2	2
Orense	-	-	-	-	-	-	-	-	9	1	0	0	9	1	0	0
Sevilla	29	7	1	2	20	12	3	4	101	29	0	2	86	34	2	10
Toledo	-	-	-	-	-	-	-	-	22	2	1	0	21	3	1	0
Valencia	-	-	-	-	-	-	-	-	16	1	1	0	14	3	0	1
Zaragoza	13	5	0	1	13	5	0	1	39	14	0	2	29	20	2	4

Table S4: The original results of under-65 classifications